Cluster Burst Synchronization in A Scale-Free Network of Inhibitory Bursting Neurons

Sang-Yoon Kim* and Woochang Lim†
Institute for Computational Neuroscience and Department of Science Education, Daegu National University of Education, Daegu 42411, Korea

We consider a scale-free network of inhibitory Hindmarsh-Rose (HR) bursting neurons, and investigate coupling-induced burst synchronization by varying the average coupling strength J_0. When passing a lower threshold J_l^*, a transition from desynchronization to 3-cluster burst synchronization occurs due to a constructive role of inhibition to favor the cluster burst synchronization. For this case, the whole population is segregated into 3 clusters, and HR neurons in each cluster exhibit burst synchronization. However, as J_0 is increased and passes an intermediate threshold J_m^*, HR neurons begin to make intermittent hoppings between the 3 clusters. Due to the intermittent intercluster hoppings, the 3 clusters are integrated into a single one. In spite of break-up of the 3 clusters, burst synchronization persists in the whole population, which is well visualized in the raster plot of burst onset times where bursting stripes (composed of burst onset times and indicating burst synchronization) appear successively. With further increase in J_0, intercluster hoppings are intensified, and bursting stripes also become smeared more and more due to a destructive role of inhibition to spoil the burst synchronization. Eventually, when passing a higher threshold J_h^* a transition to desynchronization occurs via complete overlap between the bursting stripes. Finally, we also investigate the effects of stochastic noise on both 3-cluster burst synchronization and intercluster hoppings.

PACS numbers: 87.19.lm, 87.19.lc
Keywords: Cluster burst synchronization, Intercluster hoppings, Bursting neurons, Scale-free network

I. INTRODUCTION

Recently, much attention has been paid to burst synchronization in a population of bursting neurons [1–33]. Burstings occur when neuronal activity alternates, on a slow timescale, between a silent phase and an active (bursting) phase of fast repetitive spikings [34–39]. Due to a repeated sequence of spikes in the bursting, there are several hypotheses on the importance of bursting activities in neural computation [34, 40–43]. For example, (a) bursts are necessary to overcome the synaptic transmission failure, (b) bursts are more reliable than single spikes in evoking responses in post-synaptic neurons, (c) bursts evoke long-term potentiation/depression (and hence affect synaptic plasticity much greater than single spikes), and (d) bursts can be used for selective communication between neurons. Intrinsically bursting neurons and chattering neurons in the cortex [44, 45], thalamic relay neurons and thalamic reticular neurons in the thalamus [46–48], hippocampal pyramidal neurons [49], Purkinje cells in the cerebellum [50], pancreatic β-cells [51–53], and respiratory neurons in pre-Botzinger complex [54, 55] are representative examples of bursting neurons.

Here, we are concerned about burst synchronization (i.e., synchrony on the slow bursting timescale) which characterizes temporal coherence between the burst onset times (i.e., times at which burstings start in active phases). This kind of burst synchronization is related to neural information processes in health and disease. For example, large-scale burst synchronization occurs in the sleep spindles through interaction between the excitatory thalamic relay cells and the inhibitory thalamic reticular neurons in the thalamus during the early stage of slow-wave sleep [56, 57]. These sleep spindles are associated with memory consolidation [58, 59]. In contrast, burst synchronization is also correlated to abnormal pathological rhythms, related to neural diseases such as movement disorder (Parkinson's disease and essential tremor) [60–64] and epileptic seizure [64, 65].

In addition to burst synchronization, we are also interested in cluster synchronization. For this case, the whole population is segregated into synchronous subpopulations (called also as clusters) with phase lag among them [66, 67]. This type of cluster synchronization has been investigated experimentally, numerically, or theoretically in a variety of contexts in diverse coupled (physical, chemical, biological, and neural) oscillators; to name a few, Josepson junction arrays [68, 69], globally-coupled chemical oscillators [70–72], synthetic genetic networks [73], and globally-coupled networks of inhibitory (non-oscillatory) reticular thalamic nucleus neurons [1] and other inhibitory model neurons [8, 24].

Synaptic connectivity in neural networks has been found to have complex topology which is neither regular nor completely random [74–82]. Particularly, neural networks have been found to exhibit power-law degree distributions (i.e., scale-free property) in the rat hippocampal networks [83–86] and the human cortical functional network [87]. Moreover, robustness against simulated lesions of mammalian cortical anatomical networks [88–93]

*Electronic address: sykim@icn.re.kr
†Electronic address: wclim@icn.re.kr

has also been found to be most similar to that of a scale-free network (SFN) [94]. This type of SFNs are inhomogeneous ones with a few "hubs" (i.e., superconnected nodes) [95, 96]. Many recent works on various subjects of neurodynamics have been done in SFNs with a few percent of hub neurons with an exceptionally large number of synapses [13, 14, 16, 17, 21, 29].

In this paper, we consider an inhibitory SFN of suprathreshold (i.e., self-oscillating) Hindmarsh-Rose (HR) bursting neurons, and investigate coupling-induced burst synchronization by changing the average coupling strength J_0. For sufficiently small J_0, desynchronized states exist. But, when passing a lower threshold J_l^*, a transition to 3-cluster burst synchronization occurs due to a constructive role of inhibition to favor the cluster burst synchronization. This type of cluster burst synchronization is in contrast to that occurring via post-inhibitory rebound (PIR) in globally-coupled networks of subthreshold (i.e., non-oscillating) neurons with inhibitory synaptic connections [1, 8, 24]; for the case of PIR, complete synchronization appears in each cluster (i.e., states of all the neurons in each cluster are the same). For our case, the whole population is segregated into 3 clusters. In each cluster, HR neurons make burstings every 3rd cycle of the instantaneous whole-population burst rate $R_w(t)$ of the whole population, and hence a single peak appears at 3 T_G [T_G : global period of $R_w(t)$] in the inter-burst-interval (IBI) histogram for the whole population of HR neurons. Moreover, these burstings in each cluster are also made in a coherent way, and hence a type of incomplete synchronization occurs in each cluster (i.e., burstings in each cluster show some coherence, although they are not completely synchronized). In this way, 3-cluster burst synchronization emerges. However, as J_0 is increased and passes an intermediate threshold J_m^*, HR neurons begin to make intermittent hoppings between the 3 clusters, because they intermittently fire burstings at a 4th cycle of $R_w(t)$ via burst skipping rather than at its 3rd cycle. As a result of such burst skippings, the IBI histogram is composed of two peaks at 3 T_G and 4 T_G. Due to the intermittent intercluster hoppings, the 3 clusters are integrated into a single one. However, in spite of break-up of the 3 clusters, burst synchronization persists in the whole population, which is well visualized in the raster plot of burst onset times where bursting stripes (composed of burst onset times and representing burst synchronization) appear successively. With further increase in J_0, intercluster hoppings are intensified (e.g., for a larger J_0 a 3rd peak appears at 5 T_G in the IBI histogram), and bursting stripes also become smeared more and more due to a destructive role of inhibition to spoil the burst synchronization. Eventually, when passing a higher threshold J_h^*, a transition to desynchronization occurs via complete overlap between the bursting stripes. For a desynchronized case, burst onset times are completely scattered without forming any stripes in the raster plot. Finally, the effects of stochastic noise on both 3-cluster burst synchronization and intercluster hoppings are also investigated.

This paper is organized as follows. In Sec. II, we describe a Barabási-Albert SFN composed of inhibitory HR bursting neurons. Then, in Sec. III we investigate coupling-induced burst synchronization by varying the average coupling strength J_0, and then study the effects of stochastic noise on burst synchronization in Sec. IV. Finally, we give summary and discussion in Sec. V.

II. INHIBITORY SCALE-FREE NETWORK OF HINDMARSH-ROSE BURSTING NEURONS

We consider an inhibitory SFN composed of N bursting neurons equidistantly placed on a one-dimensional ring of radius $\frac{N}{2\pi}$. We employ a directed Barabási-Albert SFN model (i.e. growth and preferential directed attachment) [95, 96]. At each discrete time t, a new node is added, and it has l_{in} incoming (afferent) edges and l_{out} outgoing (efferent) edges via preferential attachments with l_{in} (pre-existing) source nodes and l_{out} (pre-existing) target nodes, respectively. The (pre-existing) source and target nodes i (which are connected to the new node) are preferentially chosen depending on their out-degrees $d_i^{(out)}$ and in-degrees $d_i^{(in)}$ according to the attachment probabilities $\Pi_{source}(d_i^{(out)})$ and $\Pi_{target}(d_i^{(in)})$, respectively:

$$\Pi_{source}(d_i^{(out)}) = \frac{d_i^{(out)}}{\sum_{j=1}^{N_{t-1}} d_j^{(out)}} \quad \text{and}$$
$$\Pi_{target}(d_i^{(in)}) = \frac{d_i^{(in)}}{\sum_{j=1}^{N_{t-1}} d_j^{(in)}}, \tag{1}$$

where N_{t-1} is the number of nodes at the time step $t-1$. Here, we consider the case of symmetric preferential attachment with $l_{in} = l_{out}[\equiv l^*(= 15)]$. For generation of an SFN with N nodes, we begin with the initial network at $t = 0$, consisting of $N_0 = 50$ nodes where the node 1 is connected bidirectionally to all the other nodes, but the remaining nodes (except the node 1) are sparsely and randomly connected with a low probability $p = 0.1$. The processes of growth and preferential attachment are repeated until the total number of nodes becomes N. For this case, the node 1 will be grown as the head hub with the highest degree.

As an element in our SFN, we choose the representative bursting HR neuron model which was originally introduced to describe the time evolution of the membrane potential for the pond snails [97–99]. We consider the Barabási-Albert SFN composed of N HR bursting neurons. The following equations (2)-(4) govern the pop-

TABLE I: Parameter values used in our computations.

(1)	Single HR Bursting Neurons [100]				
	$a = 1$	$b = 3$	$c = 1$	$d = 5$	$r = 0.001$
	$s = 4$	$x_0 = -1.6$			
(2)	External Stimulus to HR Bursting Neurons				
	$I_{DC,i} \in [1.3, 1.4]$	D: Varying			
(3)	Inhibitory Synapse Mediated by The $\mathrm{GABA_A}$ Neurotransmitter [101]				
	$\tau_l = 1$	$\tau_r = 0.5$	$\tau_d = 5$	$X_{syn} = -2$	
(4)	Synaptic Connections between Neurons in The Barabási-Albert SFN				
	$l^* = 15$ (symmetric preferential attachment)				
	J_0 : Varying	$\sigma_0 = 0.1$			

ulation dynamics in the SFN:

$$\frac{dx_i}{dt} = y_i - ax_i^3 + bx_i^2 - z_i + I_{DC,i} + D\xi_i - I_{syn,i}, \quad (2)$$

$$\frac{dy_i}{dt} = c - dx_i^2 - y_i, \quad (3)$$

$$\frac{dz_i}{dt} = r\left[s(x_i - x_o) - z_i\right], \quad (4)$$

where

$$I_{syn,i} = \frac{1}{d_i^{(in)}} \sum_{j=1(j\neq i)}^{N} J_{ij} w_{ij} g_j(t)(x_i - X_{syn}), \quad (5)$$

$$g_j(t) = \sum_{f=1}^{F_j} E(t - t_f^{(j)} - \tau_l);$$

$$E(t) = \frac{1}{\tau_d - \tau_r}(e^{-t/\tau_d} - e^{-t/\tau_r})\Theta(t). \quad (6)$$

Here, the state of the ith neuron at a time t (measured in units of milliseconds) is characterized by three state variables: the fast membrane potential x_i, the fast recovery current y_i, and the slow adaptation current z_i. The parameter values used in our computations are listed in Table I. More details on external stimulus to each HR neuron, synaptic currents, and numerical integration of the governing equations are given in the following subsections.

A. External Stimulus to Each HR Neuron

Each bursting HR neuron (whose parameter values are in the 1st item of Table I [100]) is stimulated by a DC current $I_{DC,i}$ and an independent Gaussian white noise ξ_i [see the 5th and the 6th terms in Eq. (2)] satisfying $\langle \xi_i(t) \rangle = 0$ and $\langle \xi_i(t)\ \xi_j(t') \rangle = \delta_{ij}\ \delta(t - t')$, where $\langle \cdots \rangle$ denotes the ensemble average. The intensity of noise ξ_i is controlled by the parameter D. As I_{DC} passes a threshold $I_{DC}^* (\simeq 1.26)$ in the absence of noise (i.e., $D = 0$),

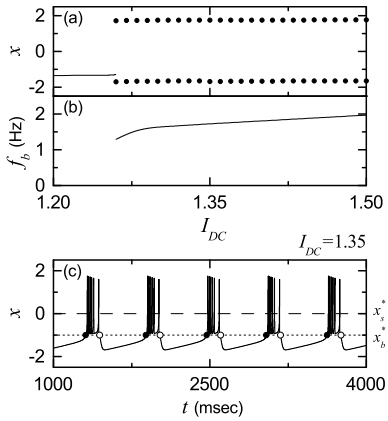

FIG. 1: Single bursting HR neuron for $D = 0$. (a) Bifurcation diagram in the single HR neuron. Solid line represents a stable resting state, while for the bursting state, maximum and minimum values of the membrane potential x are denoted by solid circles. (b) Bursting frequency f_b versus I_{DC}. (c) Time series of $x(t)$ for the bursting state when $I_{DC} = 1.35$. The dotted horizontal line ($x_b^* = -1$) and the dashed horizontal line ($x_s^* = 0$) denote the bursting and spiking thresholds, respectively. The solid and open circles represent the burst onset and offset times, respectively.

each single HR neuron exhibits a transition from a resting state to a bursting state [see Fig. 1(a)]. With increasing I_{DC}, the bursting frequency f_b, (corresponding to the reciprocal of the average IBI $\langle IBI \rangle$), increases monotonically, as shown in Fig. 1(b). For a suprathreshold case of $I_{DC} = 1.35$, deterministic bursting occurs when neuronal activity alternates, on a slow time scale ($\simeq$ 578 msec), between a silent phase and an active (bursting) phase of fast repetitive spikings, as shown in Fig. 1(c). The dotted horizontal line ($x_b^* = -1$) denotes the bursting threshold (the solid and open circles denote the active phase onset and offset times, respectively), while the dashed horizontal line ($x_s^* = 0$) represents the spiking threshold within the active phase. An active phase of the bursting activity begins (ends) at a burst onset (offset) time when the membrane potential x of the bursting HR neuron passes the bursting threshold of $x_b^* = -1$ from below (above). For this case, the HR neuron exhibits bursting activity with the slow bursting frequency f_b ($\simeq$ 1.7 Hz) [corresponding to the reciprocal of the average IBI ($\langle IBI \rangle \simeq$ 578 msec)]. Throughout this paper, we consider a suprathreshold case such that the value of $I_{DC,i}$ is chosen via uniform random sampling in the range of [1.3,1.4], as shown in the 2nd item of Table I

B. Synaptic Currents

The last term in Eq. (2) represents the synaptic couplings of HR bursting neurons. The coupling strength of the synapse from the jth pre-synaptic neuron to the ith post-synaptic neuron is J_{ij}. These synaptic strengths

are normally distributed with the mean J_0 and the standard deviation σ_0 ($= 0.1$). $I_{syn,i}$ of Eq. (5) represents a synaptic current injected into the ith neuron, and X_{syn} is the synaptic reversal potential. The synaptic connectivity is given by the connection weight matrix W ($=\{w_{ij}\}$) where $w_{ij} = 1$ if the bursting neuron j is presynaptic to the bursting neuron i; otherwise, $w_{ij} = 0$. Here, the synaptic connection is modeled in terms of the Barabási-Albert SFN. Then, the in-degree of the ith neuron, $d_i^{(in)}$ (i.e., the number of synaptic inputs to the neuron i) is given by $d_i^{(in)} = \sum_{j=1(j\neq i)}^{N} w_{ij}$. The fraction of open synaptic ion channels at time t is denoted by $g(t)$. The time course of $g_j(t)$ of the jth neuron is given by a sum of delayed double-exponential functions $E(t - t_f^{(j)} - \tau_l)$ [see Eq. (6)], where τ_l is the synaptic delay, and $t_f^{(j)}$ and F_j are the fth spike and the total number of spikes of the jth neuron at time t, respectively. Here, $E(t)$ [which corresponds to contribution of a presynaptic spike occurring at time 0 to $g_j(t)$ in the absence of synaptic delay] is controlled by the two synaptic time constants: synaptic rise time τ_r and decay time τ_d, and $\Theta(t)$ is the Heaviside step function: $\Theta(t) = 1$ for $t \geq 0$ and 0 for $t < 0$. For the inhibitory GABAergic synapse (involving the $\mathrm{GABA_A}$ receptors), the values of τ_l, τ_r, τ_d, and X_{syn} are listed in the 3rd item of Table I [101].

C. Numerical Integration

Numerical integration of differential equations (2)-(4) is done by using the 4th-order Runge-Kutta method in the absence of noise ($D = 0$) and the Heun method [102] in the presence of noise ($D > 0$) (with the time step $\Delta t = 0.01$ msec). For each realization, we choose a random initial point $[x_i(0), y_i(0), z_i(0)]$ for the ith ($i = 1, \ldots, N$) neuron with uniform probability in the range of $x_i(0) \in (-1.5, 1.5)$, $y_i(0) \in (-10, 0)$, and $z_i(0) \in (1.2, 1.5)$.

III. COUPLING-INDUCED BURST SYNCHRONIZATION OF HR BURSTING NEURONS

In this section, we consider a directed Barabási-Albert SFN with the symmetric attachment degree $l^* = 15$, composed of N inhibitory HR bursting neurons. The synaptic coupling strengths $\{J_{ij}\}$ are chosen from the Gaussian distribution with the mean J_0 and the standard deviation σ_0 ($= 0.1$). We investigate coupling-induced burst synchronization by varying J_0 in the absence of noise ($D = 0$).

A. Emergence of Cluster Burst Synchronization

Burst synchronization in the whole population may be well visualized in the raster plot of burst onset times

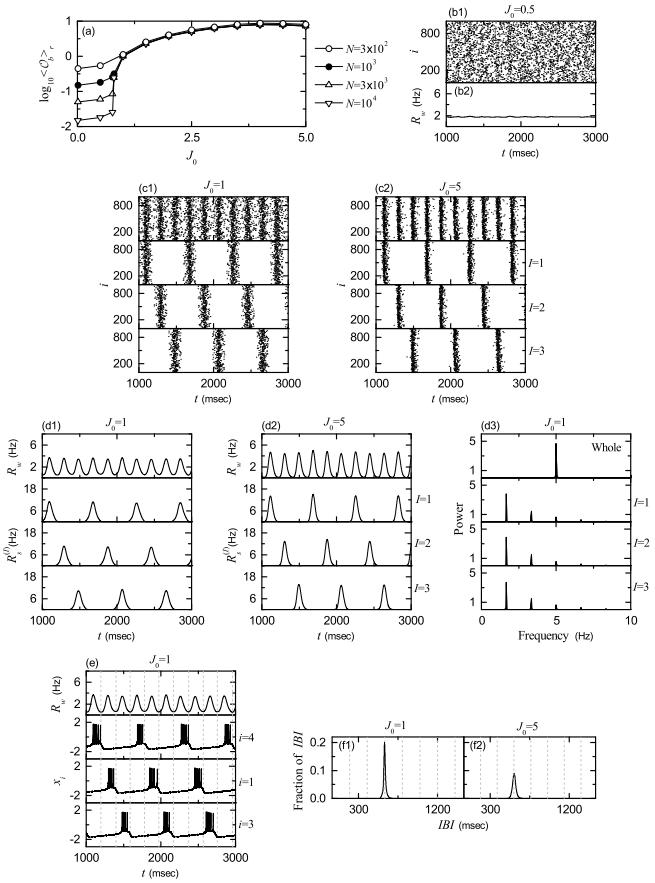

FIG. 2: 3-cluster burst synchronization for $D = 0$; $N = 10^3$ except for the case of (a). (a) Plots of thermodynamic bursting order parameter $\langle \mathcal{O}_b \rangle_r$ versus the average coupling strength J_0. (b1) Raster plot of burst onset times and (b2) IWPBR kernel estimate $R_w(t)$ in the case of desynchronization for $J_0 = 0.5$. Raster plots of burst onset times in the whole population and the I th cluster ($I = 1$, 2, and 3) when $J_0 =$ (c1) 1 and (c2) 5. IWPBR kernel estimate $R_w(t)$ of the whole population and ISPBR kernel estimate $R_s^{(I)}(t)$ of the Ith cluster ($I = 1$, 2, and 3) for $J_0 =$ (d1) 1 and (d2) 5. (d3) One-sided power spectra of $\Delta R_w(t)$ $[= R_w(t) - \overline{R_w(t)}]$ (top panel) and $\Delta R_s^{(I)}(t)$ $[= R_s^{(I)}(t) - \overline{R_s^{(I)}(t)}]$ ($I = 1$, 2, and 3 panels) with the mean-squared amplitude normalization. (e) Time series of membrane potential $x_i(t)$ of a representative neuron in each cluster; i =4, 1, and 3 for $I = 1$, 2, and 3 clusters, respectively. IWPBR kernel estimate $R_w(t)$ is also given on the top panel, and the dotted vertical lines represent its global cycles. IBI histograms for $J_0 =$ (f1) 1 and (f2) 5. Vertical dotted lines in (f1) and (f2) denote the integer multiples of the global period T_G of $R_w(t)$.

which corresponds to a collection of all trains of burst onset times of individual bursting neurons. For the case of burst synchronization, bursting stripes (composed of burst onset times and representing burst synchronization) appear successively in the raster plot [e.g., see the top panel of Fig. 2(c1) for $J_0 = 1$], while in the desynchronized case burst onset times are completely scattered

without forming any bursting stripes [e.g., see Fig. 2(b1) for $J_0 = 0.5$]. To see emergence of burst synchronization in the whole population, we employ an (experimentally-obtainable) instantaneous whole population burst rate (IWPBR) which is often used as a collective quantity showing bursting behaviors. This IWPBR may be obtained from the raster plot of burst onset times [30–33]. To obtain a smooth IWPBR, we employ the kernel density estimation (kernel smoother) [103]. Each burst onset time in the raster plot is convoluted (or blurred) with a kernel function $K_h(t)$ to obtain a smooth estimate of IWPBR $R_w(t)$:

$$R_w(t) = \frac{1}{N} \sum_{i=1}^{N} \sum_{b=1}^{n_i} K_h(t - t_b^{(i)}), \tag{7}$$

where $t_b^{(i)}$ is the bth burst onset time of the ith neuron, n_i is the total number of burst onset times for the ith neuron, and we use a Gaussian kernel function of band width h:

$$K_h(t) = \frac{1}{\sqrt{2\pi}h} e^{-t^2/2h^2}, \qquad -\infty < t < \infty \tag{8}$$

Throughout the paper, the band width h of $K_h(t)$ is 20 msec. In the case of burst synchronization, the IWPBR kernel estimate $R_w(t)$ shows a slow-wave oscillation with a whole-population bursting frequency $f_b^{(w)}$ [e.g., see the top panel of Fig. 2(d1) for $J_0 = 1$]. In contrast, for a desynchronized case $R_w(t)$ is nearly stationary [e.g., see Fig. 2(b2) for $J_0 = 0.5$].

Recently, we introduced a realistic bursting order parameter, based on $R_w(t)$, for describing transition from desynchronization to burst synchronization [31]. The mean square deviation of $R_w(t)$,

$$\mathcal{O}_b \equiv \overline{(R_w(t) - \overline{R_w(t)})^2}, \tag{9}$$

plays the role of an order parameter $\mathcal{O}_b$; the overbar represents the time average. This bursting order parameter may be regarded as a thermodynamic measure because it concerns just the macroscopic IWPBR kernel estimate $R_w(t)$ without any consideration between $R_w(t)$ and microscopic individual burst onset times. As N (number of HR neurons in the whole population) is increased, $R_w(t)$ exhibits more regular oscillations for the case of burst synchronization, while $R_w(t)$ becomes more stationary in the case of desynchronization. Hence, in the thermodynamic limit of $N \to \infty$, the bursting order parameter $\mathcal{O}_b$, representing time-averaged fluctuations of $R_w(t)$ from its time-averaged mean, approaches a non-zero (zero) limit value for the synchronized (desynchronized) state. In this way, the bursting order parameter $\mathcal{O}_b$ can determine whether population states are synchronized or desynchronized.

Figure 2(a) shows a plot of $\log_{10}\langle\mathcal{O}_b\rangle_r$ versus J_0. In each realization, we discard the first time steps of a trajectory as transients for 10^3 msec, and then we numerically compute $\mathcal{O}_b$ by following the trajectory for 3×10^4 msec. Hereafter, $\langle\cdots\rangle_r$ denotes an average over 20 realizations. For $J_0 < J_l^* (\simeq 0.78)$, the bursting order parameter $\langle\mathcal{O}_b\rangle_r$ tends to zero with increasing N. On the other hand, when passing J_l^* a transition to burst synchronization occurs, because $\langle\mathcal{O}_b\rangle_r$ approaches a non-zero limit value. Consequently, for $J_0 > J_l^*$ burst synchronization occurs in the whole population due to a constructive role of synaptic inhibition to favor the burst synchronization. Figures 2(b1)-2(b2) show an example of desynchronization for $J_0 = 0.5$, where burst onset times in the raster plot are completely scattered and the corresponding IWPBR kernel estimate $R_w(t)$ is nearly stationary. Two examples for burst synchronization are given for $J_0 = 1$ and 5. For the case of $J_0 = 1$, bursting stripes appear successively in the raster plot of burst onset times [see the top panel of Fig. 2(c1)], and the corresponding IWPBR kernel estimate $R_w(t)$ exhibits a slow-wave oscillation, as shown in the top panel of Fig. 2(d1). As J_0 is further increased, burst synchronization gets better, as shown for the case of $J_0 = 5$ [see top panels of Figs. 2(c2) and 2(d2)]; bursting stripes in the raster plot become clearer (i.e. less smeared) and the amplitudes of $R_w(t)$ become larger.

We note that the whole population for $J_0 = 1$ and 5 is segregated into 3 sub-populations (clusters); N_I (number of neurons in the Ith ($I = 1$, 2, and 3) cluster) $\simeq \frac{N}{3}$. This type of clustering may be well seen in the raster plots for the clusters. Bursting stripes in each cluster appear successively every 3rd global cycle of $R_w(t)$, as shown in the $I = 1$, 2, and 3 panels of Figs. 2(c1) and 2(c2). To see emergence of burst synchronization in each cluster, we employ an instantaneous sub-population burst rate (ISPBR) which is also obtained from the raster plot of burst onset times in each cluster. As in the case of $R_w(t)$, we get the ISPBR kernel estimate $R_s^{(I)}(t)$ by employing the Gaussian kernel function of Eq. (8):

$$R_s^{(I)}(t) = \frac{1}{N_I} \sum_{i=1}^{N_I} \sum_{b=1}^{n_i^{(I)}} K_h(t - t_b^{(I,i)}), \tag{10}$$

where $t_b^{(I,i)}$ is the bth burst onset time of the ith neuron in the Ith cluster, $n_i^{(I)}$ is the total number of burst onset times for the ith neuron in the Ith cluster, and N_I is the number of neurons in the Ith cluster. The ISPBR kernel estimates $R_s^{(I)}$ of the Ith clusters for $J_0 = 1$ and 5 are shown in the I =1, 2, and 3 panels of Figs. 2(d1) and 2(d2), respectively. They exhibit regular oscillations with the sub-population bursting frequency $f_b^{(I)}$.

Both the whole-population bursting frequency $f_b^{(w)}$ and the sub-population bursting frequency $f_b^{(I)}$ of the regularly-oscillating IWPBR kernel estimate $R_w(t)$ and ISPBR kernel estimate $R_s^{(I)}(t)$ may be obtained from the one-sided power spectra of $\Delta R_w(t)$ [$= R_w(t) - \overline{R_w(t)}$] and $\Delta R_s^{(I)}(t)$ [$= R_s^{(I)}(t) - \overline{R_s^{(I)}(t)}$] with the mean-squared amplitude normalization, respectively. The number of data for each power spectrum is 2^{13}, and the overline denotes

the time average. Figure 2(d3) shows power spectra of $\Delta R_w(t)$ (top panel) and $\Delta R_s^{(I)}(t)$ (I =1, 2, and 3 panels) for $J_0 = 1$. For the case of whole population, the power spectrum has its peak at $f_b^{(w)} \simeq 5$ Hz. On the other hand, in the case of each sub-population (cluster), the power spectrum has a main peak at $f_b^{(I)} \simeq \frac{f_b^{(w)}}{3}$ and its harmonics. Hence, $R_s^{(I)}(t)$ oscillates with the slow sub-population bursting frequency $f_b^{(I)}$. For $J_0 = 5$, both $f_b^{(w)}$ and $f_b^{(I)}$ are increased; $f_b^{(w)} \simeq 5.3$ Hz and $f_b^{(I)} \simeq \frac{f_b^{(w)}}{3}$.

We also investigate individual bursting behaviors of HR neurons in each cluster. Figure 2(e) shows a time series of a membrane potential $x_i(t)$ of a representative neuron in each Ith cluster (i =4, 1, and 3 for I = 1, 2, and 3, respectively), along with the IWPBR kernel estimate $R_w(t)$; the vertical dotted lines represent global cycles of $R_w(t)$. The 4th HR neuron in the $I = 1$ cluster makes burstings in the 1st global cycle of $R_w(t)$ (after the transient time $t = 10^3$ msec). We note that the duration of silent phase of the 4th neuron is about twice as long as the length of its active bursting phase. During this silent phase, the 1st and the 3rd HR neurons in the $I = 2$ and 3 clusters exhibit burstings alternately in the 2nd and the 3rd global cycles of $R_w(t)$, respectively. In this way, individual HR neurons in each cluster show burstings every 3rd global cycle of $R_w(t)$. This kind of individual bursting behaviors are well shown in the IBI histograms [see Figs. 2(f1) and 2(f2), where vertical dotted lines denote the multiples of global periods T_G of $R_w(t)$; $T_G \simeq 200.2$ and 190.5 msec for $J_0 = 1$ and 5, respectively]. Each IBI histogram is composed of 5×10^4 IBIs, and the bin size for the histogram is 2.5 msec. We note that single peaks appear at 3 T_G for both cases of $J_0 = 1$ and 5, which is also consistent with $f_b^{(I)} \simeq \frac{f_b^{(w)}}{3}$. The peak for $J_0 = 5$ is broader than that for $J_0 = 1$, because $J_0 = 5$ is close to an intermediate threshold $J_m^* (\simeq 5.2)$ where break-up of 3 clusters occurs (this point is explained in details in the following subsection).

B. Break-up of Cluter Burst Synchronization via Intercluster Hoppings

As J_0 is further increased and passes an intermediate threshold J_m^* ($\simeq 5.2$), 3-cluster burst synchronization breaks up into (non-cluster) burst synchronization without clustering through intercluster hoppings. As an example, we consider the case of $J_0 = 10$.

Figure 3(a) shows the IBI histogram with two peaks at 3 T_G and 4 T_G [T_G ($\simeq 170.5$ msec): global period of $R_w(t)$]. For $J_0 < J_m^*$, only single peak appears at 3 T_G [i.e., individual HR neurons exhibit burstings every 3rd global cycle of $R_w(t)$], as shown in Figs. 2(f1) and 2(f2). As J_0 approaches the threshold J_m^*, this peak becomes broad along with decrease in its height. After passing J_m^*, individual HR neurons begin to exhibit burstings intermittently at a 4th cycle of $R_w(t)$ through burst skipping at its 3rd cycle. Here, 3rd and 4th cycles of $R_w(t)$ refer to ones counted just after the latest burstings (e.g., see the example given below). An example for the 5th neuron in the 1st ($I = 1$) cluster is given in Fig. 3(b). A burst skipping occurs in the small box in the gray region [corresponding to a 3rd cycle of $R_w(t)$], and then another bursting appears at its 4th cycle; for reference, $R_w(t)$ is shown on the top panel and vertical dotted lines represent global cycles of $R_w(t)$. Thus, in addition to the major peak at 3 T_G, a new minor peak appears at 4 T_G in Fig. 3(a).

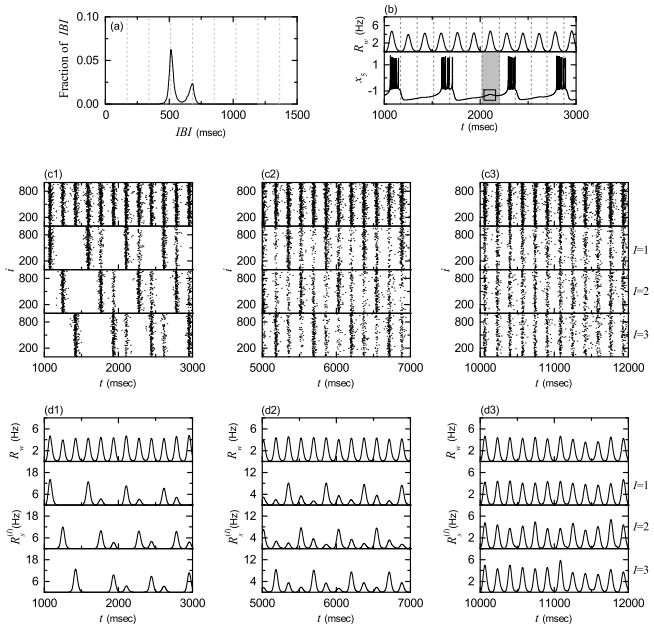

FIG. 3: Break-up of clusters via intercluster hoppings in the absence of noise ($D = 0$) for $J_0 = 10$ and $N = 10^3$. (a) Double-peaked IBI histogram. Vertical dotted lines denote integer multiples of the global period T_G ($\simeq 170.5$ msec) of $R_w(t)$. (b) Time series of membrane potential $x_5(t)$ for the 5th HR neuron in the 1st ($I = 1$) cluster. For reference, the IWPBR kernel estimate $R_w(t)$ of the whole population is shown in the top panel. The 5th HR neuron exhibits a bursting at the 4th cycle of $R_w(t)$ rather than at its 3rd cycle where it shows a hopping instead of bursting, as shown inside the small box in the gray region (corresponding to the 3rd cycle). Sequential long-term raster plots of burst onset times for the whole population and the Ith cluster (I =1, 2, and 3) in (c1) the early, (c2) the intermediate, and (c3) the final stages. IWPBR kernel estimates $R_w(t)$ of the whole population and ISPBR kernel estimates $R_s^{(I)}(t)$ of the Ith cluster (I =1, 2, and 3) in the (d1) early, (d2) the intermediate, and (d3) the final stages.

Intercluster hoppings may be well seen in sequential long-term raster plots of burst onset times in the whole population and in the Ith (I = 1, 2, and 3) clusters. Figures 3(c1)-3(c3) show such raster plots, corresponding to (c1) the early, (c2) the intermediate, and (c3) the final stages. For the initial stage in Fig. 3(c1), individ-

ual HR neurons in the Ith cluster make intermittent intercluster hoppings to the nearest neighboring $(I+1)$th cluster (i.e., neurons in the Ith cluster exhibit intermittent burstings at a 4th cycle of $R_w(t)$ (along with regular burstings of neurons in the $(I+1)$th cluster) due to burst skipping at its 3rd cycle). As a result, additional bursting stripes (composed of intermittent burstings occurring at a 4th cycle of $R_w(t)$ due to burst skipping at its 3rd cycle) appear next to the regular bursting stripes in the raster plot for the Ith cluster. These additional bursting stripes in the Ith cluster are vertically aligned with regular bursting stripes in the $(I+1)$th cluster. In this way, intermittent hoppings from the Ith to the $(I+1)$th clusters occur. For the intermediate stage in Fig. 3(c2), one more step occurs for the intercluster hoppings due to a 2nd burst skipping, and hence intercluster hoppings occur from the Ith cluster to the $(I+1)$th cluster (due to a 1st burst skipping) and then to the $(I+2)$th cluster (due to a 2nd burst skipping). Consequently, two successive additional bursting stripes (consisting of intermittent burstings occurring at a 4th cycle of $R_w(t)$ due to 1st and 2nd burst skippings) appear next to the regular bursting stripes in the raster plot of the Ith cluster. These two additional bursting stripes are vertically aligned with regular bursting stripes of the $(I+1)$th and the $(I+2)$th clusters. Consequently, for each cluster bursting stripes appear at every cycle of $R_w(t)$ in the raster plot, like the case of whole population, although additional bursting stripes (formed due to burst skippings) are still somewhat sparse (i.e. their densities are low in comparison with those of regular bursting stripes). As the time t is further increased, a 3rd burst skipping may also occur, and then another intercluster hopping from the $(I+2)$th to the Ith clusters occurs (i.e., return to the original Ith cluster occurs due to a 3rd burst skipping). In this way, intercluster hoppings occur in a cyclic way ($I \to I+1 \to I+2 \to I$) due to burst skippings. After a sufficiently long time, in the final stage in Fig. 3(c3), intercluster hoppings between clusters are more and more intensified, which leads to complete break-up of clusters. As a result, density of all bursting stripes becomes nearly the same, independently of $I = 1$, 2, and 3. We also note that, in spite of break-up of clusters, burst synchronization persists in the whole population, because bursting stripes appear successively in the rater plot of the whole population.

Figures 3(d1)-3(d3) show the IWPBR kernel estimates $R_w(t)$ and the ISPBR kernel estimates $R_s^{(I)}(t)$, corresponding to the above raster plots in Figs. 3(c1)-3(c3). In the initial stage in Fig. 3(d1), smaller-amplitude oscillations [corresponding to lower-density additional bursting stripes appearing due to burst skippings at regular 3rd cycles of $R_w(t)$] appear next to the regular oscillations [occurring at every 3rd cycle of $R_w(t)$] for each Ith ($I = 1$, 2, and 3) case. In the intermediate stage in Fig. 3(d2), one more step for intercluster hoppings occurs due to 2nd burst skippings, and hence two successive smaller-amplitude oscillations appear next to the regular

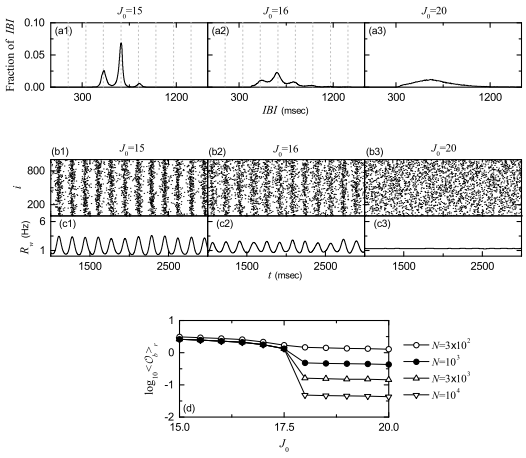

FIG. 4: Transition to desynchronization for $D = 0$; $N = 10^3$ except for the case of (d). IBI histograms for $J_0 =$ (a1) 15, (a2) 16, and (a3) 20. Vertical dotted lines denote integer multiples of the global period T_G of $R_w(t)$. Raster plots of burst onset times for $J_0 =$ (b1) 15, (b2) 16, and (b3) 20. IWPBR kernel estimates $R_w(t)$ of the whole population for $J_0 =$ (c1) 15, (c2) 16, and (c3) 20. (d) Plots of thermodynamic bursting order parameter $\langle \mathcal{O}_b \rangle_r$ versus the average coupling strength J_0.

oscillations in each Ith ($I = 1$, 2, and 3) case. Then, for each I $R_s^{(I)}(t)$ makes oscillations at every cycle of $R_w(t)$, although its amplitudes vary depending on the cycles of $R_w(t)$. As the time t is further increased, these amplitudes tend to become nearly the same due to intensified intercluster hoppings, as shown in Fig. 3(d3) for the final stage. Consequently, all the ISPBR kernel estimates $R_s^{(I)}(t)$ become nearly the same as the IWPBR kernel estimate $R_w(t)$, independently of I, because of complete break-up of clusters.

So far, we consider the case of $J_0 = 10$ where (non-cluster) burst synchronization without clustering appears via intercluster hoppings which occur due to burst skippings. With increase in J_0 from 10, another type of bursting skippings begin to occur at 4th cycles of $R_w(t)$, in addition to the above skippings at 3rd cycles for $J_0 = 10$. Figure 4(a1) shows the IBI histogram for $J_0 = 15$. When compared with the IBI histogram for $J_0 = 10$ in Fig. 3(a), the height of the peak at 4 T_G is so much increased, and hence its height becomes higher than that of the decreased peak at 3 T_G. As a result, the peak at 4 T_G becomes a major one. Furthermore, a new smaller peak appears at 5 T_G due to intermittent burst skippings at 4th cycles of $R_w(t)$. Thus, the IBI histogram for $J_0 = 15$ consists of 3 peaks at 3 T_G, 4 T_G, and 5 T_G. Figures 4(b1) and 4(c1) show the raster plot and the corresponding IWPBR kernel estimate $R_w(t)$ for $J_0 = 15$. In comparison with the case of $J_0 = 10$ in Figs. 3(c1) and 3(d1), due to s destructive role of synaptic inhibition to spoil the burst synchronization, burst stripes become more smeared, and amplitudes of $R_w(t)$ become smaller. Consequently, the degree of burst synchronization becomes worse.

As J_0 is further increased, this kind of tendency for burst skippings is intensified. As an example, see the case of $J_0 = 16$. The IBI histogram is shown in Fig. 4(a2). In comparison with the IBI histogram in Fig. 4(a1) for $J_0 = 15$, heights of both peaks at 3 T_G and 4 T_G are decreased, while the height of the peak at 5 T_G is a little increased. Additionally, a new small peak appears at 6 T_G. In this way, the IBI distribution becomes broad. When compared with the case of $J_0 = 15$, bursting stripes become more smeared and amplitudes of $R_w(t)$ are decreased, as shown in Figs. 4(b2) and 4(c2), respectively. In this way, with increasing J_0 burst synchronization becomes more and more worse.

Eventually, when passing a higher threshold J_h^* ($\simeq$ 17.8), a transition to desynchronization occurs. Consequently, for $J_0 > J_h^*$ desynchronized states appear, as shown in the case of $J_0 = 20$. For this case, the IBI histogram is so broad and has just a central maximum via merging of peaks. Burst onset times in the raster plot are completely scattered without forming any bursting stripes, and the corresponding IWPBR kernel estimate $R_w(t)$ becomes nearly stationary [see Figs. 4(b3) and 4(c3), respectively]. This type of transition from burst synchronization to desynchronization may also be well described in terms of the bursting order parameter $\mathcal{O}_b$ of Eq. (9). Figure 4(d) shows a plot of $\log_{10}\langle\mathcal{O}_b\rangle_r$ versus J_0. As N is increased, the bursting order parameter $\langle\mathcal{O}_b\rangle_r$ approaches a non-zero limit value for $J_0 < J_h^*(\simeq 17.8)$, and hence burst synchronization occurs. On the other hand, when passing J_h^* a transition to desynchronization occurs, because $\langle\mathcal{O}_b\rangle_r$ tends to zero with increasing N. Consequently, for $J_0 > J_h^*$ desynchronized states appear due to a destructive role of synaptic inhibition to spoil the burst synchronization.

C. Characterization of Burst Synchronization

We characterize burst synchronization in the range of $J_l^* < J_0 < J_h^*$ by employing a statistical-mechanical bursting measure M_b [31]. For the case of burst synchronization, bursting stripes appear successively in the raster plot of burst onset times. The bursting measure $M_i^{(b)}$ of the ith bursting stripe is defined by the product of the occupation degree $O_i^{(b)}$ of burst onset times (representing the density of the ith bursting stripe) and the pacing degree $P_i^{(b)}$ of burst onset times (denoting the smearing of the ith bursting stripe):

$$M_i^{(b)} = O_i^{(b)} \cdot P_i^{(b)}. \tag{11}$$

The occupation degree $O_i^{(b)}$ of burst onset times in the ith bursting stripe is given by the fraction of bursting neurons:

$$O_i^{(b)} = \frac{N_i^{(b)}}{N}, \tag{12}$$

where $N_i^{(b)}$ is the number of bursting neurons in the ith bursting stripe. In the case of full burst synchronization, all bursting neurons exhibit burstings in each bursting stripe in the raster plot of burst onset times, and hence the occupation degree $O_i^{(b)}$ of Eq. (12) in each bursting stripe becomes 1. On the other hand, for the case of sparse burst synchronization, only some fraction of bursting neurons show burstings in each bursting stripe, and hence the occupation degree $O_i^{(b)}$ becomes less than 1. For our case of burst synchronization, $O_i^{(b)} < 1$ in the range of $J_l^* < J_0 < J_h^*$, and hence sparse burst synchronization occurs. The pacing degree $P_i^{(b)}$ of burst onset times in the ith bursting stripe can be determined in a statistical-mechanical way by taking into account their contributions to the macroscopic IWPBR kernel estimate $R_w(t)$. Central maxima of $R_w(t)$ between neighboring left and right minima of $R_w(t)$ coincide with centers of bursting stripes in the raster plot. A global cycle starts from a left minimum of $R_w(t)$, passes a maximum, and ends at a right minimum. An instantaneous global phase $\Phi^{(b)}(t)$ of $R_w(t)$ was introduced via linear interpolation in the region forming a global cycle (for more details, refer to Eqs. (14) and (15) in [31]). Then, the contribution of the kth microscopic burst onset time in the ith bursting stripe occurring at the time $t_k^{(b)}$ to $R_w(t)$ is given by $\cos\Phi_k^{(b)}$, where $\Phi_k^{(b)}$ is the global phase at the kth burst onset time [i.e., $\Phi_k^{(b)} \equiv \Phi^{(b)}(t_k^{(b)})$]. A microscopic burst onset time makes the most constructive (in-phase) contribution to $R_w(t)$ when the corresponding global phase $\Phi_k^{(b)}$ is $2\pi n$ ($n = 0, 1, 2, \dots$), while it makes the most destructive (anti-phase) contribution to $R_w(t)$ when $\Phi_k^{(b)}$ is $2\pi(n - 1/2)$. By averaging the contributions of all microscopic burst onset times in the ith bursting stripe to $R_w(t)$, we obtain the pacing degree of burst onset times in the ith stripe:

$$P_i^{(b)} = \frac{1}{B_i}\sum_{k=1}^{B_i} \cos\Phi_k^{(b)}, \tag{13}$$

where B_i is the total number of microscopic burst onset times in the ith stripe. By averaging $M_i^{(b)}$ of Eq. (11) over a sufficiently large number N_b of bursting stripes, we obtain the realistic statistical-mechanical bursting measure M_b, based on the IWPBR kernel estimate $R_w(t)$:

$$M_b = \frac{1}{N_b}\sum_{i=1}^{N_b} M_i^{(b)}. \tag{14}$$

We follow 3×10^3 bursting stripes in each realization and get $\langle M_b\rangle_r$ via average over 20 realizations. Figures 5(a)-5(c) show the average occupation degree $\langle\langle O_i^{(b)}\rangle\rangle_r$, the average pacing degree $\langle\langle P_i^{(b)}\rangle\rangle_r$, and the statistical-mechanical bursting measure $\langle M_b\rangle_r$, respectively. For the case of 3-cluster burst synchronization in the range of J_l^* ($\simeq 0.78$) $< J_0 < J_m^*$ ($\simeq 5.2$), $\langle\langle O_i^{(b)}\rangle\rangle_r$ (denoting

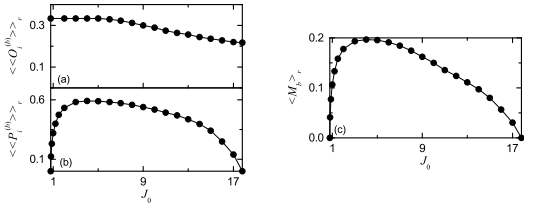

FIG. 5: Characterization of burst synchronization for $D = 0$. Plots of (a) the average occupation degree $\langle\langle O_i^{(b)}\rangle\rangle_r$, (b) the average pacing degree $\langle\langle P_i^{(b)}\rangle\rangle_r$, and (c) the statistical-mechanical bursting measure $\langle M_b\rangle_r$ versus the average coupling strength J_0.

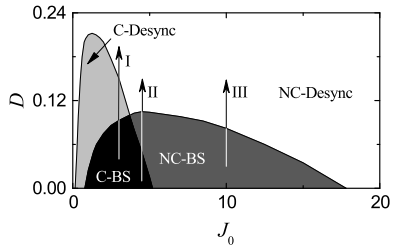

FIG. 6: State diagram in the $J_0 - D$ plane. Four types of population states exist. 3-cluster burst synchronization occurs in the black region,denoted by $C - BS$, while non-cluster burst synchronization occurs in the dark gray region, represented by $NC - BS$. Cluster desynchronization appears in the gray region, denoted by $C - Desync$, while non-cluster desynchronization appears in the remaining white region, represented by $NC - Desync$. Vertical arrows (I, II, and III) represent routes for $J_0 = 3$, 4.5, and 10 where effects of stochastic noise are studied.

the density of bursting stripes in the raster plot) is $\frac{1}{3}$, because individual HR neurons exhibit burstings every 3rd cycle of $R_w(t)$. However, for $J_0 > J_m^*$, $\langle\langle O_i^{(b)}\rangle\rangle_r$ decreases slowly to a limit value ($\simeq 0.217$), due to burst skippings [e.g., see IBI histograms Figs. 4(a1) and 4(a2)]. The average pacing degree $\langle\langle P_i^{(b)}\rangle\rangle_r$ represents well the average smearing of bursting stripes in the raster plot of burst onset times [e.g., see Figs. 2(c1), 2(c2), 4(b1), and 4(b2)]. As J_0 is increased from J_l^*, $\langle\langle P_i^{(b)}\rangle\rangle_r$ increases rapidly to a maximum ($\simeq 0.591$) for $J_0 \simeq 4.0$ (i.e., the degree of 3-cluster burst synchronization increases rapidly after its appearance). Then, for $J_0 > 4$ it decreases to zero at the higher transition point J_h^* ($\simeq 17.8$) (i.e., decrease in $\langle\langle P_i^{(b)}\rangle\rangle_r$ begins a little before break-up of 3-cluster burst synchronization for $J_0 = J_m^*$, and then $\langle\langle P_i^{(b)}\rangle\rangle_r$ decreases smoothly to zero, due to complete overlap of sparse bursting stripes). Through product of the average occupation and pacing degrees of burst onset times, the statistical-mechanical bursting measure $\langle M_b\rangle_r$ is obtained. Since the variation in $\langle\langle O_i^{(b)}\rangle\rangle_r$ is small, $\langle M_b\rangle_r$ behaves like the case of $\langle\langle P_i^{(b)}\rangle\rangle_r$. With increasing J_0 from J_l^*, $\langle M_b\rangle_r$ increases rapidly to a maximum ($\simeq 0.197$) for $J_0 \simeq 4.0$, and then, for $J_0 > 4$ it decreases slowly to zero at the higher transition point J_h^*

IV. EFFECTS OF STOCHASTIC NOISE ON BURST SYNCHRONIZATION

In this section, we study the effects of stochastic noise on burst synchronization by changing the noise intensity D. First, we obtain the state diagram in the $J_0 - D$ plane, which is shown in Fig. 6. Four types of population states exist. 3-cluster states appear in the gray region, denoted by C, on the left side. Also, burst synchronization occurs in the dark gray region, represented by BS, on the right side. In the intersection region, shaded in black and denoted by $C - BS$, between the cluster and the burst synchronization regions, 3-cluster burst synchronization occurs. On the other hand, in the remaining regions of the cluster and the burst synchronization regions, cluster desynchronization and non-cluster burst synchronization occurs, respectively; these remaining regions are denoted by $C - Desync$ and $NC - BS$, respectively. Outside these cluster and burst synchronization regions, non-cluster desynchronization occurs in a region denoted by $NC - Desync$.

Next, we investigate the effects of noise on 3-cluster burst synchronization and intercluster hoppings (studied in the above section for $D = 0$) by increasing the noise intensity D along the 3 routes for J_0 =3, 4.5, and 10, denoted by vertical arrows (I, II, and III) in the state diagram of Fig. 6.

A. Effects of Noise in The Route I

Figure 7 shows results on the noise effects in the 1st route I for $J_0 = 3$. For $D = 0$ a 3-cluster burst synchronization occurs. As D is increased and passes a lower threshold D_l^* ($\simeq 0.093$), a transition to desynchronization occurs, which may be described in terms of the bursting order parameter $\mathcal{O}_b$ of Eq. (9). Figure 7(a) shows a plot of $\log_{10}\langle\mathcal{O}_b\rangle_r$ versus D. With increasing N, the bursting order parameter $\langle\mathcal{O}_b\rangle_r$ approaches a non-zero limit value for $0 \le D < D_l^*$, and hence burst synchronization occurs. On the other hand, when passing D_l^* a transition to desynchronization occurs, because $\langle\mathcal{O}_b\rangle_r$ tends to zero, as N is increased. Consequently, for $D > D_l^*$ desynchronized states appear due to a destructive role of noise to spoil the burst synchronization.

This kind of transition from 3-cluster burst synchronization to desynchronization may also be well seen in the raster plots of burst onset times in the whole population and in the Ith clusters (I =1, 2, and 3). Figures 7(b1)-7(b5) show such raster plots for D =0, 0.04, 0.06, 0.08, and 0.12, respectively. Their corresponding IWPBR kernel estimates $R_w(t)$ and the ISPBR kernel estimates $R_s^{(I)}(t)$ are also given in Figs. 7(c1)-7(c5) when D =0, 0.04, 0.06, 0.08, and 0.12, respectively. For $D = 0$, burst-

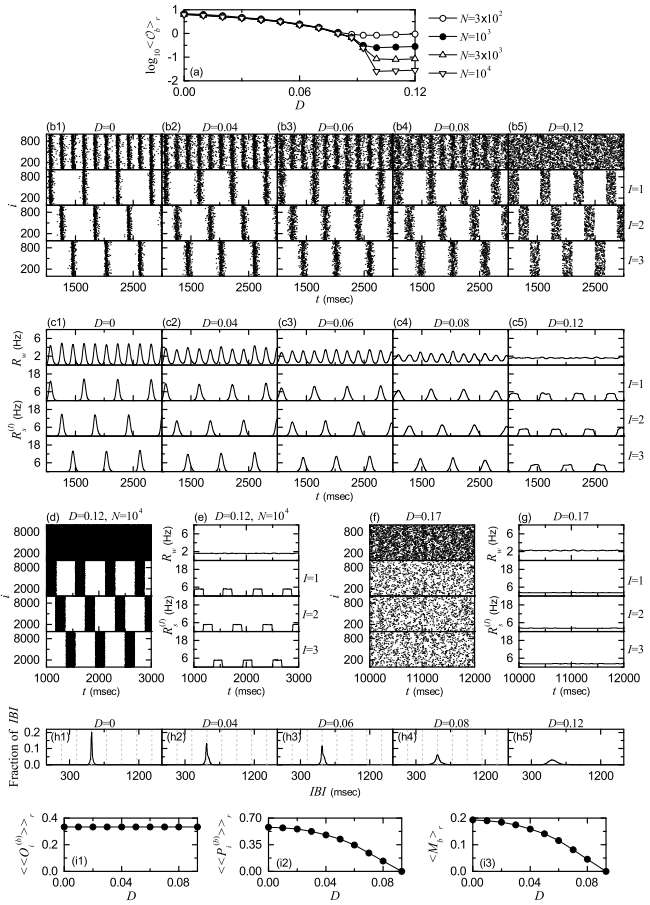

FIG. 7: Noise effect in the 1st route for $J_0 = 3$; $N = 10^3$ except for the cases of (a), (d) and (e). (a) Plots of thermodynamic bursting order parameter $\langle \mathcal{O}_b \rangle_r$ versus the noise intensity D. Raster plots of burst onset times in the whole population and in the I th cluster ($I = 1$, 2, and 3) when $D =$ (b1) 0, (b2) 0.04, (b3) 0.06, (b4) 0.08, and (b5) 0.12. IWPBR kernel estimates $R_w(t)$ of the whole population and ISPBR kernel estimates $R_s^{(I)}(t)$ of the Ith cluster ($I = 1$, 2, and 3) for $D =$ (c1) 0, (c2) 0.04, (c3) 0.06, (c4) 0.08, and (c5) 0.12. (d) Raster plots of burst onset times in the whole population and in the I th cluster ($I = 1$, 2, and 3) for $D = 0.12$ and $N = 10^4$. (e) IWPBR kernel estimate $R_w(t)$ of the whole population and ISPBR kernel estimates $R_s^{(I)}(t)$ of the Ith cluster ($I = 1$, 2, and 3) for $D = 0.12$ and $N = 10^4$. (f) Raster plots of burst onset times in the whole population and in the I th cluster ($I = 1$, 2, and 3) for $D = 0.17$. (g) IWPBR kernel estimate $R_w(t)$ of the whole population and ISPBR kernel estimates $R_s^{(I)}(t)$ of the Ith cluster ($I = 1$, 2, and 3) for $D = 0.17$. IBI histograms for $D =$ (h1) 0, (h2) 0.04, (h3) 0.06, (h4) 0.08, and (h5) 0.12. Vertical dotted lines in (h1)-(h4) denote the integer multiples of the global period T_G of $R_w(t)$. Plots of (i1) the average occupation degree $\langle \langle O_i^{(b)} \rangle \rangle_r$, (i2) the average pacing degree $\langle \langle P_i^{(b)} \rangle \rangle_r$, and (i3) the statistical-mechanical bursting measure $\langle M_b \rangle_r$ versus D.

ing stripes (representing burst synchronization) appear successively in the raster plot for the whole population [see the top panel of Fig. 7(b1)], and the corresponding IWPBR kernel estimate $R_w(t)$ exhibits a slow-wave oscillation with the whole-population frequency $f_b^{(w)}$ ($\simeq 5.2$ Hz), as shown in the top panel of Fig. 7(c1). The whole population is segregated into 3 clusters (I =1, 2, and 3), which is well seen in the raster plots for the clusters [see the $I = 1$, 2, and 3 panels in Fig. 7(b1)]. We note that bursting stripes in each cluster appear successively every 3rd cycle of $R_w(t)$, and the corresponding ISPBR kernel estimate $R_s^{(I)}(t)$ exhibits a regular oscillation with the sub-population frequency $f_b^{(I)}$ ($\simeq \frac{f_b^{(w)}}{3}$). In this way, 3-cluster burst synchronization appears for $D = 0$. For this case, a single peak appears at 3 T_G [T_G ($\simeq 193.4$ msec): global period of $R_w(t)$] in the IBI histogram, as shown in Fig. 7(h1).

As D is increased from 0, the 3-cluster burst synchronization for $D = 0$ persists, but its degree becomes more and more worse due to a destructive role of noise to spoil the burst synchronization. As shown in Figs. 7(b2)-7(b4), with increasing D, bursting stripes in the whole population and in each Ith ($I = 1$, 2, and 3) cluster become smeared more and more. Hence, amplitudes of $R_w(t)$ and $R_s^{(I)}(t)$ also decrease, as D is increased [see Figs. 7(c2)-7(c4)]. The IBI histograms also become broader (along with decrease in their heights), with increasing D [see Figs. 7(h2)-7(h4)].

Eventually, when passing a lower threshold D_l^*, a transition to desynchronization occurs. Consequently, desynchronized states appear for $D > D_l^*$. As an example, see the raster plots in Fig. 7(b5) and the IWPBR kernel estimate $R_w(t)$ and the ISPBR kernel estimates $R_s^{(I)}(t)$ in Fig. 7(c5) for $D = 0.12$. Burst onset times in the raster plot for the whole population seem to be completely scattered, and the corresponding IWPBR kernel estimate $R_w(t)$ is nearly stationary.

However, we note that, for $D = 0.12$ bursting bands in the raster plot for each cluster are preserved, and the corresponding ISPBR kernel estimate $R_s^{(I)}(t)$ shows a square-wave-like behavior. For each cluster, burst onset times in each bursting band are nearly completely scattered (i.e., nearly desynchronized), and hence a square-wave-like oscillation occurs in each $R_s^{(I)}(t)$. During the "silent" part (without burstings) for about $\frac{2P}{3}$, $R_s^{(I)}(t) = 0$ (which corresponds to the bottom part), while in the bursting band for about $\frac{P}{3}$, $R_s^{(I)}(t)$ rapidly increases to the nearly flat top, and then decreases rapidly; P ($\simeq 573.6$ msec) corresponds to the average period of the square-wave oscillation. Through repetition of this process $R_s^{(I)}(t)$ exhibits a square-wave-like oscillation. For this case, the IBI histogram in Fig. 7(h5) becomes broader in comparison with those for the cases of burst synchronization, and its average IBI $\langle IBI \rangle$ is 573.7 msec (corresponding to the above period P). To examine the square-wave-like behavior more clearly, the

number of HR neurons is increased from $N = 10^3$ to 10^4. For this case, raster plots for the whole population and the clusters and their corresponding IWPBR kernel estimate $R_w(t)$ and the ISPBR kernel estimates $R_s^{(I)}(t)$ are shown in Figs. 7(d) and 7(e), respectively. For the whole population, burst onset times are more completely scattered, and hence the corresponding IWPBR kernel estimate $R_w(t)$ is more stationary. Furthermore, for each cluster bursting bands in the raster plot show clearly the clustering structure, and hence the corresponding ISPBR kernel estimate $R_s^{(I)}(t)$ shows square-wave oscillations more clearly. Thus, for each cluster burst onset times in bursting bands are completely scattered, and they show a desynchronized state. In this way, 3-cluster desynchronization appears, as D passes D_l^*.

However, as D is further increased and passes a higher threshold D_h^* ($\simeq 0.15$), clusters are broken up via inter-cluster hoppings due to another destructive role of noise to break up the clusters. Hence, for $D > D_h^*$ non-cluster desynchronized states appear. As an example, we consider the case of $D = 0.17$. For this case, raster plots and the corresponding IWPBR kernel estimate $R_w(t)$ and ISPBR kernel estimate $R_s^{(I)}(t)$ are shown in Figs. 7(f) and 7(g), respectively. We note that raster plots in the $I = 1$, 2, and 3 panels show no clustered bursting bands. These raster plots where burst onset times are completely scattered without forming clusters are essentially the same, independently of I. As a result, all of $R_w(t)$ and $R_s^{(I)}(t)$ are nearly stationary. In this way, for $D > D_h^*$ non-cluster desynchronization occurs.

Figures 7(i1)-7(i3) show the average occupation degree $\langle\langle O_i^{(b)}\rangle\rangle_r$ of Eq. (12) (representing the average density of bursting stripes), the average pacing degree $\langle\langle P_i^{(b)}\rangle\rangle_r$ of Eq. (13) (denoting the average smearing of bursting stripes), and the statistical-mechanical bursting measure $\langle M_b\rangle_r$ of Eq. (14) (given by the product of occupation and pacing degrees), respectively, in the range of $0 \le D < D_l^*$ where 3-cluster burst synchronization occurs. Obviously, $\langle\langle O_i^{(b)}\rangle\rangle_r = \frac{1}{3}$, because 3-clusters persist for $0 \le D < D_l^*$. Due to a destructive role of noise to spoil the burst synchronization, as D is increased from 0 to D_l^*, $\langle\langle P_i^{(b)}\rangle\rangle_r$ decreases smoothly from 0.581 to zero. Then, the statistical-mechanical bursting measure $\langle M_b\rangle_r$ also makes a smooth decrease from 0.194 to 0, as in the case of $\langle\langle P_i^{(b)}\rangle\rangle_r$, because $\langle\langle O_i^{(b)}\rangle\rangle_r$ is constant.

B. Effects of Noise in The Route II

As J_0 is increased and passes a threshold J^{**} ($\simeq 3.7$), break-up of clusters in the desynchronized states (e.g., the above route I case for $J_0 = 3$) no longer occurs. Instead, before a transition to desynchronization, break-up of clusters occurs in the burst-synchronized states. As an example, see the route II for $J_0 = 4.5$ in Fig. 6. Figure 8 shows results on the noise effects in the 2nd route

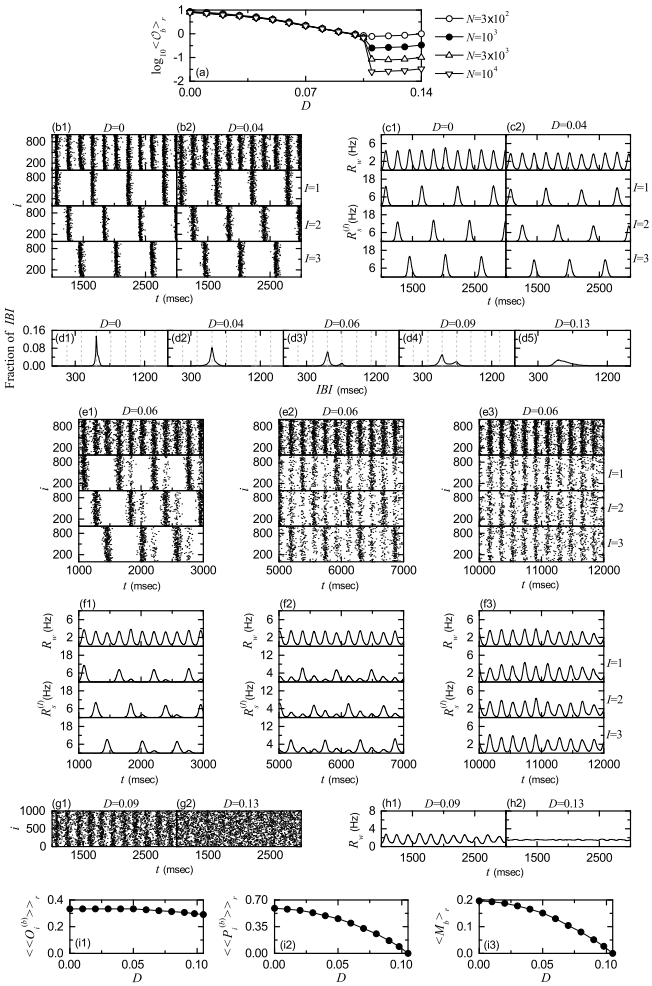

FIG. 8: Noise effect in the 2nd route for $J_0 = 4.5$; $N = 10^3$ except for the case of (a). (a) Plots of thermodynamic bursting order parameter $\langle\mathcal{O}_b\rangle_r$ versus the noise intensity D. Raster plots of burst onset times in the whole population and in the Ith cluster ($I = 1$, 2, and 3) when $D =$ (b1) 0 and (b2) 0.04. IWPBR kernel estimates $R_w(t)$ of the whole population and ISPBR kernel estimates $R_s^{(I)}(t)$ of the Ith cluster ($I = 1$, 2, and 3) for $D =$ (c1) 0 and (c2) 0.04. IBI histograms for $D =$ (d1) 0, (d2) 0.04, (d3) 0.06, (d4) 0.09, and (d5) 0.13. Vertical dotted lines in (d1)-(d4) denote the integer multiples of the global period T_G of $R_w(t)$. For $D = 0.06$, sequential long-term raster plots of burst onset times for the whole population and the clusters in (e1) the early, (e2) the intermediate, and (e3) the final stages. For $D = 0.06$, $R_w(t)$ of the whole population and $R_s^{(I)}(t)$ of the clusters in the (f1) early, (f2) the intermediate, and (f3) the final stages. Raster plots of burst onset times in the whole population for $D =$ (g1) 0.09 and (g2) 0.13. $R_w(t)$ of the whole population for $D =$ (h1) 0.09 and (h2) 0.13. Plots of (i1) the average occupation degree $\langle\langle O_i^{(b)}\rangle\rangle_r$, (i2) the average pacing degree $\langle\langle P_i^{(b)}\rangle\rangle_r$, and (i3) the statistical-mechanical bursting measure $\langle M_b\rangle_r$ versus D.

II for $J_0 = 4.5$. With increasing D, noise first breaks up clusters, and then a transition to desynchronization occurs due to another destructive role of noise to spoil the burst synchronization. Hence, the destructive roles of D is similar to those of J_0, shown in Figs. 3-4 in the absence of noise ($D = 0$).

The bursting order parameter $\mathcal{O}_b$ of Eq. (9) may describe well a transition from burst synchronization to desynchronization. Figure 8(a) shows a plot of $\log_{10}\langle\mathcal{O}_b\rangle_r$ versus D. As N is increased, the bursting order parameter $\langle\mathcal{O}_b\rangle_r$ approaches a non-zero limit value for $0 \le D < D_h^{**}$ ($\simeq 0.105$), and hence burst synchronization occurs. In contrast, when passing D_h^{**} a transition to desynchronization occurs, because $\langle\mathcal{O}_b\rangle_r$ tends to zero, with increasing N. Consequently, for $D > D_h^{**}$ desynchronized states appear due to a destructive role of noise to spoil the burst synchronization.

As in the 1st route I for $J_0 = 3$, when $D = 0$ appearance of 3-cluster burst synchronization is well shown in the raster plots for the whole population and the clusters ($I = 1$, 2, and 3) [see Fig. 8(b1)] and their corresponding IWPBR kernel estimate $R_w(t)$ and the ISPBR kernel estimates $R_s^{(I)}(t)$ [see Fig. 8(c1)]. For each cluster, bursting stripes appear every 3rd cycle of $R_w(t)$, which results in emergence of 3-cluster burst synchronization. For this case, the IBI histogram has a single peak at 3 T_G [T_G : global period of $R_w(t)$], as shown in Fig. 8(d1). As D is increased, bursting stripes in the raster plots become smeared, due to a destructive role of noise to spoil the burst synchronization, and hence amplitudes of $R_w(t)$ and $R_s^{(I)}(t)$ are decreased [e.g., see Figs. 8(b2) and 8(c2) for $D = 0.04$]. In this case, the IBI histogram has a broad single peak with lower height at 3 T_G, as shown in Fig. 8(d2).

Eventually, as D passes a lower threshold D_l^{**} ($\simeq 0.05$), the IBI histogram begins to have a new minor peak at 4 T_G, in addition to the major peak at 3 T_G, as shown in Fig. 8(d3). Hence, individual HR neurons begin to exhibit burstings intermittently at a 4th cycle of $R_w(t)$ via burst skipping at its 3rd cycle. Due to burst skippings, clusters become broken up via intercluster hoppings, as in the case of Fig. 3 for $J_0 = 10$ in the absence of noise ($D = 0$). As a result, (non-cluster) burst synchronization without clustering appears in the whole population. As an example, we consider the case of $D = 0.06$. Similar to the case in Figs. 3(c1)-3(c3) and Figs. 3(d1)-3(d3), intercluster hoppings for $D = 0.06$ are well seen in sequential long-term raster plots of burst onset times in the whole population and in the Ith ($I = 1$, 2, and 3) clusters [see Figs. 8(e1)-8(e3)] and in the corresponding IWPBR kernel estimates $R_w(t)$ of the whole population and the ISPBR kernel estimates $R_s^{(I)}(t)$ of the clusters [see Figs. 8(f1)-8(f3)]. Here, Figs. 8(e1) and 8(f1), Figs. 8(e2) and 8(f2), and Figs. 8(e3) and 8(f3) show the initial, the intermediate, and the final stages, respectively. With increasing the stage, intercluster hoppings are more and more intensified due to burst skippings, which results in complete break-up of clusters. Thus, after a sufficiently long time, raster plots in the cluster ($I = 1$, 2, and 3) are essentially the same, irrespectively of I. Although clusters are broken up, bursting stripes persist, and hence burst synchronization without clustering occurs in the whole population.

With increasing D from 0.06, the degree of burst synchronization is decreased due to a destructive role of noise to spoil the burst synchronization. In the IBI histogram for $D = 0.09$, the height of the peak at 3 T_G is decreased, while the height of the peak at 4 T_G increases a little [see Fig. 8(d4)]. Thus, the IBI histogram becomes broader, and burst skippings are enhanced. Consequently, intercluster hoppings are more intensified. Figures 8(g1) and 8(h1) show the raster plot and the corresponding IWPBR kernel estimate $R_w(t)$ for $D = 0.09$, respectively. In comparison with the case of $D = 0.06$, bursting stripes are more smeared and amplitudes of $R_w(t)$ are decreased. Eventually, when passing the threshold D_h^{**} ($\simeq 0.105$), a transition from non-cluster burst synchronization to desynchronization occurs. Then, for $D > D_h^{**}$ desynchronized states appear. As an example of desynchronized state, we consider the case of $D = 0.13$. With increasing D the two peaks in the IBI histogram for $D = 0.09$ are merged, and then it has a broad single maximum, as shown in Fig. 8(d5) for $D = 0.13$. For this case, burst onset times are completely scattered in the raster plot, and the corresponding IWPBR kernel estimate $R_w(t)$ is nearly stationary [see Figs. 8(g2) and 8(h2)].

Figures 8(i1)-8(i3) show the average occupation degree $\langle\langle O_i^{(b)}\rangle\rangle_r$ (denoting the average density of bursting stripes), the average pacing degree $\langle\langle P_i^{(b)}\rangle\rangle_r$ (representing the average smearing of bursting stripes), and the statistical-mechanical bursting measure $\langle M_b\rangle_r$ (given by the product of occupation and pacing degrees), respectively, in the range of $0 \le D < D_h^{**}$ where burst synchronization occurs. In the range of $0 \le D < D_l^{**}$, 3-cluster burst synchronization appears, and hence $\langle\langle O_i^{(b)}\rangle\rangle_r = \frac{1}{3}$. However, as a result of break-up of clusters, for $D > D_l^{**}$, $\langle\langle O_i^{(b)}\rangle\rangle_r$ decreases slowly to a limit value ($\simeq 0.291$) for $D = D_h^{**}$, due to bursting skippings. With increasing D from 0 to D_h^{**}, bursting stripes become more and more smeared due to a destructive role of noise to spoil the burst synchronization, and eventually they become completely overlapped for $D = D_h^{**}$. Hence, in the range of $0 \le D < D_h^{**}$, $\langle\langle P_i^{(b)}\rangle\rangle_r$ decreases smoothly from 0.587 to zero. Then, through product of the average occupation and pacing degrees of burst onset times, the statistical-mechanical bursting measure $\langle M_b\rangle_r$ also makes a smooth decrease from 0.196 to 0, like the case of $\langle\langle P_i^{(b)}\rangle\rangle_r$, because variations in $\langle\langle O_i^{(b)}\rangle\rangle_r$ are small.

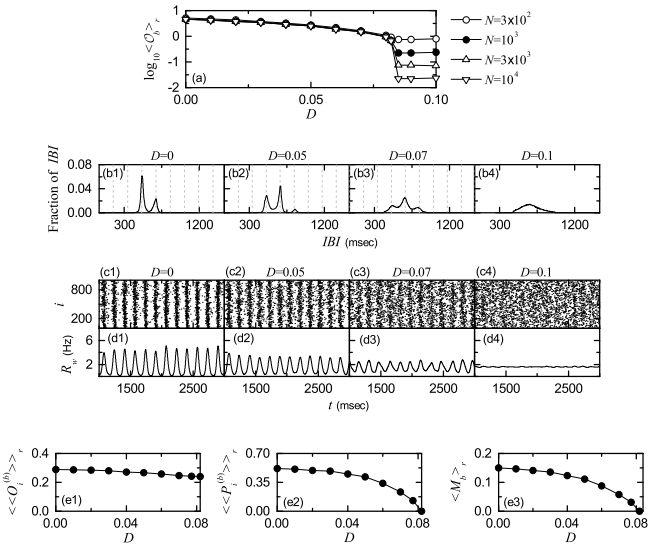

FIG. 9: Noise effect in the 3rd route for $J_0 = 10$; $N = 10^3$ except for the case of (a). (a) Plots of thermodynamic bursting order parameter $\langle \mathcal{O}_b \rangle_r$ versus the noise intensity D. IBI histograms for $D =$ (b1) 0, (b2) 0.05, (b3) 0.07, and (b4) 0.1. Vertical dotted lines in (b1)-(b3) represent the integer multiples of the global period T_G of $R_w(t)$. Raster plots of burst onset times in the whole population when $D =$ (c1) 0, (c2) 0.05, (c3) 0.07, and (c4) 0.1. IWPBR kernel estimates $R_w(t)$ of the whole population for $D =$ (d1) 0, (d2) 0.05, (d3) 0.07, and (d4) 0.1. Plots of (e1) the average occupation degree $\langle\langle O_i^{(b)} \rangle\rangle_r$, (e2) the average pacing degree $\langle\langle P_i^{(b)} \rangle\rangle_r$, and (e3) the statistical-mechanical bursting measure $\langle M_b \rangle_r$ versus D.

C. Effects of Noise in The Route III

Finally, we consider the route III for $J_0 = 10$ in Fig. 6. Unlike the above cases of routes I and II, in the absence of noise ($D = 0$) clusters are broken up due to burst skippings, and hence (non-cluster) burst synchronization without clustering appears. In this case, we investigate the noise effect on the non-cluster burst synchronization by increasing D, and due to destructive roles of noise, both intensified intercluster hoppings via burst skippings and smearing of bursting stripes are thus found.

As shown in the above cases, a transition from burst synchronization to desynchronization may be well described in terms of the bursting order parameter $\mathcal{O}_b$. Figure 9(a) shows a plot of $\log_{10}\langle \mathcal{O}_b \rangle_r$ versus D. With increasing N, the bursting order parameter $\langle \mathcal{O}_b \rangle_r$ converges to a non-zero limit value for $0 \le D < D^{***}$ ($\simeq 0.082$). Consequently, burst synchronization occurs. On the other hand, when passing D^{***} a transition to desynchronization occurs, because $\langle \mathcal{O}_b \rangle_r$ tends to zero, as N is increased. Accordingly, for $D > D^{***}$ desynchronized states appear due to a destructive role of noise to spoil the burst synchronization.

Figures 9(b1)-9(b4) show the IBI histograms for D =0, 0.05, 0.07, and 0.1, respectively. For $D = 0$, a minor peak appears at 4 T_G, in addition to the major peak at 3 T_G. Hence, individual HR neurons exhibit burstings intermittently at a 4th cycle of $R_w(t)$ via burst skipping at its 3rd cycle. Due to this type of burst skippings, interbursting hoppings occur between clusters, and the clusters become broken up. Thus, for $D = 0$ (non-cluster) burst synchronization without clustering appears, in contrast to the above two cases.

With increasing D, the height of the peak at 4 T_G is increased, while the height of the peak at 3 T_G decreases. Furthermore, a small peak also appears at 5 T_G, as shown in Fig. 9(b2) for $D = 0.05$. Hence, intercluster hoppings become intensified due to enhanced burst skippings. With further increase in D, these 3 peaks begin to show a tendency of merging [e.g., see Fig. 9(b3) for $D = 0.07$]. In the desynchronized case of $D = 0.1$, these peaks are completely merged, and then the IBI histogram has a broad single peak.

Figures 9(c1)-9(c4) show raster plots for $D = 0$, 0.05, 0.07, and 0.1, respectively, and their corresponding IWPBR kernel estimates $R_w(t)$ are also shown in Figs. 9(d1)-9(d4), respectively. As D is increased from 0, bursting stripes in the raster plots become more and more smeared, and amplitudes of $R_w(t)$ also are decreased. Hence, with increasing D the degree of burst synchronization becomes worse, due to a destructive role of noise to spoil the burst synchronization.

Figures 9(e1)-9(e3) show the average occupation degree $\langle\langle O_i^{(b)} \rangle\rangle_r$, the average pacing degree $\langle\langle P_i^{(b)} \rangle\rangle_r$, and the statistical-mechanical bursting measure $\langle M_b \rangle_r$ respectively, in the range of $0 \le D < D^{***}$ where burst synchronization (without clustering) occurs. As D is increased from 0 to D^{***}, burst skippings become intensified, and hence $\langle\langle O_i^{(b)} \rangle\rangle_r$ decreases smoothly from 0.289 (for $D = 0$) to 0.241 (for $D = D^{***}$). With increasing D from 0 to D^{***}, bursting stripes become more and more smeared due to a destructive role of noise to spoil the burst synchronization, and eventually they become completely overlapped for $D = D^{***}$. Hence, in the range of $0 \le D < D^{***}$, $\langle\langle P_i^{(b)} \rangle\rangle_r$ decreases smoothly from 0.516 to zero. Then, through product of the average occupation and pacing degrees of burst onset times, the statistical-mechanical bursting measure $\langle M_b \rangle_r$ also makes a smooth decrease from 0.149 to 0, as in the case of $\langle\langle P_i^{(b)} \rangle\rangle_r$, because variations in $\langle\langle O_i^{(b)} \rangle\rangle_r$ are small.

V. SUMMARY AND DISCUSSION

We investigated coupling-induced burst synchronization by changing the average coupling strength J_0 in an inhibitory Barabási-Albert SFN of HR bursting neurons. For sufficiently small J_0, desynchronized states exist. But, as J_0 passes a lower threshold J_l^* ($\simeq 0.78$), a transition to 3-cluster burst synchronization has been found to occur due to a constructive role of inhibition to favor the cluster burst synchronization. In each clus-

ter, HR neurons make burstings every 3rd cycle of the IWPBR kernel estimate $R_w(t)$. Therefore, a single peak has been found to appear at 3 T_G [T_G : global period of $R_w(t)$] in the IBI histogram. Furthermore, these burstings in each cluster have been found to exhibit burst synchronization. In this way, 3-cluster burst synchronization has been found to emerge. Burst synchronization in the whole population may be well visualized in the raster plot of burst onset times where bursting stripes appear in a regular and successive way, and the corresponding IWPBR kernel estimate $R_w(t)$ shows regular oscillations with the whole-population bursting frequency $f_b^{(w)}$. Moreover, cluster synchronization may also be seen well in the raster plot of burst onset times in each cluster, along with the corresponding ISPBR kernel estimate $R_s^{(I)}(t)$ (I =1, 2, and 3) of the sub-populations. Bursting stripes in each cluster appear every 3rd cycle of $R_w(t)$, and the corresponding ISPBR kernel estimate $R_s^{(I)}(t)$ exhibits regular oscillations with the sub-population bursting frequency $f_s^{(I)}$ ($\simeq \frac{f_b^{(w)}}{3}$).

However, with increase in J_0 and passing an intermediate threshold J_m^* ($\simeq 5.2$), HR neurons have been found to exhibit intermittent hoppings between the 3 clusters, since they intermittently fire burstings at a 4th cycle of $R_w(t)$ due to burst skipping rather than at its 3rd cycle, and hence the IBI histogram is composed of two peaks at 3 T_G and 4 T_G. As a result of the intermittent intercluster hoppings, the 3 clusters have been found to be integrated into a single one, which was well shown in sequential long-term raster plots of burst onset times. Although the 3 clusters are broken up, burst synchronization has been found to persist in the whole population. As J_0 is further increased, intercluster hoppings have been found to be intensified due to enhanced burst skippings (e.g., for $J_0 = 15$ a 3rd peak appears at 5 T_G in the IBI histogram), and bursting stripes have also been found to be smeared more and more because of a destructive role of inhibition to spoil the burst synchronization. Eventually, as a higher threshold J_h^* ($\simeq 17.8$) is passed, a transition to desynchronization has been found to occur. Then, burst onset times are completely scattered in the raster plot due to complete overlap between the bursting stripes, and the IWPBR kernel estimate $R_w(t)$ becomes nearly stationary.

In the above way, through competition between the constructive and the destructive roles of synaptic inhibition, burst synchronization has been found to occur in an intermediate range of $J_l^* < J_0 < J_h^*$. Particularly, when passing J_l^*, 3-cluster burst synchronization emerges due to a constructive role of inhibition to favor the cluster burst synchronization. However, with increasing J_0 and passing an intermediate threshold J_m^*, it is transformed into (non-cluster) burst synchronization without clustering via intercluster hoppings due to a destructive role of inhibition to break up clusters. As J_0 is further increased and passes a higher threshold J_h^*, a transition to desynchronization occurs because of another destructive role of inhibition to spoil the burst synchronization.

We have also studied the effects of stochastic noise on burst synchronization, and obtained a state diagram in the $J_0 - D$ plane. By increasing the noise intensity D, we investigated the noise effects along the 3 routes I, II, and III for $J_0 = 3$, 4.5, and 10. For $J_l^* < J_0 < J_m^*$ (where 3-cluster burst synchronization occurs for $D = 0$), two cases have been found to appear; the 1st (2nd) case occurs when $J_0 < (>) J^{**} (\simeq 3.7)$. As the 1st example, we considered the 1st route I for $J_0 = 3$. With increasing D, bursting stripes become just smeared (without intercluster hoppings) due to a destructive role of noise to spoil the cluster burst synchronization. Eventually when passing a lower threshold D_l^* ($\simeq 0.093$), a transition from the 3-cluster burst synchronization to desynchronization has been found to occur via complete overlap between the bursting stripes. As a result, desynchronized 3-cluster states appear for $D > D_l^*$. However, as D is further increased and passes a higher threshold $D_h^* (\simeq 0.15)$, the 3 clusters have been found to be broken up via intercluster hoppings due to a destructive role of noise to break up the clusters, and then (non-cluster) desynchronized states without clustering appear for $D > D_h^*$. On the other hand, in the 2nd route II for $J_0 = 4.5$, intercluster hoppings have been found to occur before desynchronization when passing a lower threshold $D_l^{**} (\simeq 0.05)$ due to a destructive role of noise to break up the clusters, in addition to smearing of bursting stripes. Hence, for $D > D_l^{**}$ (non-cluster) burst synchronization without clustering persists in the whole population, in contrast to the 1st example. Then, a transition to (non-cluster) desynchronization has been found to occur when passing a higher threshold $D_h^{**} (\simeq 0.105)$. As a 3rd example, we considered the 3rd route III for $J_0 = 10$ (where (non-cluster) burst synchronization without clustering exists for $D = 0$). With increasing D from 0, both smearing and intercluster hoppings have been found to be intensified due to a destructive role of noise, and when passing a threshold D^{***} ($\simeq 0.082$), (non-cluster) desynchronized states have been found to occur. As shown in these 3 examples, the stochastic noise plays destructive dual roles to spoil the burst synchronization and to break up clusters. We also note that, in the present work in a population of (self-firing) suprathreshold bursting neurons, noise makes just destructive effects on population states without showing any constructive role. These noise effects for the suprathreshold case are in contrast to those in previous works [30, 33] on stochastic burst synchronization (SBS) in a population of (non-self-firing) subthreshold bursting neurons where SBS was found to appear in an intermediate range of noise intensity via competition between the constructive and the destructive roles of noise.

Finally, we expect that our results on burst synchronization, associated with neural information processes in health and disease, would make some contributions for understanding mechanisms of emergence and break-up of cluster burst synchronization and effects of stochastic

noise on burst synchronization.

Acknowledgments

This research was supported by the Basic Science Research Program through the National Research Foundation of Korea (NRF) funded by the Ministry of Education (Grant No. 20162007688).

[1] D. Golomb and J. Rinzel, Physica D **72**, 259 (1994).
[2] R. C. Elson, A. I. Selverston, R. Huerta, N. F. Rulkov, M. I. Rabinovich, and H. D. I. Abarbanel, Phys. Rev. Lett. **81**, 5691 (1998).
[3] E. A. Stern, D. Jaeger, and C. J. Wilson, Nature **394**, 475 (1998).
[4] P. Varona, J. J. Torres, H. D. I. Abarbanel, M. I. Rabinovych, and R. C. Elson, Biol. Cybern. **84**, 91 (2001).
[5] C. van Vreeswijk and D. Hansel, Neural Comput. **13**, 959 (2001).
[6] M. Dhamala, V. Jirsa, and M. Ding, Phys. Rev. Lett. **92**, 028101 (2004).
[7] M. V. Ivanchenko, G. Osipov, V. Shalfeev, and J. Kurths, Phys. Rev. Lett. **93**, 134101 (2004).
[8] D. T. W. Chik, S. Coombes, and Z. D. Wang, Phys. Rev. E **70**, 011908 (2004).
[9] A. Shilnikov and G. Cymbalyuk, Phys. Rev. Lett. **94**, 048101 (2005).
[10] X. Shi and Q. Lu, Chinese Phys. **14**, 77 (2005).
[11] G. Tanaka, B. Ibarz, M.A. Sanjuan, and K. Aihara, Chaos **16**, 013113 (2006).
[12] T. Pereira, M. Baptista, and J. Kurths, Eur. Phys. J. Spec. Top. **146**, 155 (2007).
[13] C. A. S. Batista, A.M. Batista, J. A. C. de Pontes, R. L. Viana, and S. R. Lopes, Phys. Rev. E **76**, 016218 (2007).
[14] C. A. S. Batista, A. M. Batista, J. C. A. de Pontes, S. R. Lopes, and R. L. Viana, Chaos Soliton. Fract. **41**, 2220 (2009).
[15] X. Shi and Q. Lu, Physica A **388**, 2410 (2009).
[16] Q. Wang, M. Perc, Z. Duan, and G. Chen, Phys. Rev. E **80**, 026206 (2009).
[17] C. A. S. Batisa, S. R. Lopes, R. L. Viana, and A. M. Batisa, Neural Netw. **23**, 114 (2010).
[18] X. Sun, J. Lei, M. Perc, J. Kurths, and G. Chen, Chaos **21**, 016110 (2011).
[19] H. Yu, J. Wang, B. Deng, X. Wei, Y. K. Wong, W. L. Chan, K.M. Tsang, and Z. Yu, Chaos **21**, 013127 (2011).
[20] Q.-Y. Wang, A. Murks, M. Perc, and Q.-S. Lu, Chinese Phys. B **20**, 040504 (2011).
[21] Q. Wang, G. Chen, and M. Perc, PLoS ONE **6**, e15851 (2011).
[22] C. A. Batista, E. L. Lameu, A. M. Batista, S. R. Lopes, T. Pereira, G. Zamora-Lopez, J. Kurths, and R. L. Viana, Phys. Rev. E **86**, 016211 (2012).
[23] E. L. Lameu, C. A. S. Batista, A. M. Batista, K. Larosz, R. L. Viana, S. R. Lopes, and J. Kurths, Chaos **22**, 043149 (2012).
[24] A. J. Langdon, M. Breakspear, and S. Coombes, Phys. Rev. E **86**, 061903 (2012).
[25] L. Duan, D. Fan, and Q. Lu, Cogn. Neurodyn. **7**, 341 (2013).
[26] P. Meng, Q. Wang, and Q. Lu, Cogn. Neurodyn. **7**, 197 (2013).
[27] H. Wang, Q. Wang, Q. Lu, and Y. Zheng, Cogn. Neurodyn. **7**, 121 (2013).
[28] T. de L. Prado, S. R. Lopes, C. A. S. Batista, J. Kurths, and R. L. Viana, Phys. Rev. E **90**, 032818 (2014).
[29] B. A. S. Ferrari, R. L. Viana, S. R. Lopes, and R. Stoop, Neural Netw. **66**, 107 (2015).
[30] S.-Y. Kim and W. Lim, Cogn. Neurodyn. **9**, 179 (2015).
[31] S.-Y. Kim and W. Lim, Physica A **438**, 544 (2015).
[32] S.-Y. Kim and W. Lim, Neural Netw. **79**, 53 (2016).
[33] S.-Y. Kim and W. Lim, Cogn. Neurodyn. **12**, 315 (2018).
[34] E. M. Izhikevich, Scholarpedia **1(3)**, 1300 (2006).
[35] E. M. Izhikevich, Int. J. Bifurcat. Chaos **10**, 1171 (2000).
[36] *Bursting: The Genesis of Rhythm in the Nervous System,* edited by S. Coombes and P. C. Bressloff (World Scientific, Singapore, 2005).
[37] J. Rinzel, in *Ordinary and Partial Differential Equations*, edited by B. D. Sleeman and R. J. Jarvis, Lecture Notes in Mathematics Vol. 1151 (Springer, Berlin, 1985), pp. 304-316.
[38] J. Rinzel, in *Mathematical Topics in Population Biology, Morphogenesis, and Neurosciences*, edited by E. Teramoto and M. Yamaguti, Lecture Notes in Biomathematics Vol. 71 (Springer, Berlin, 1987), pp. 267-281.
[39] E. M. Izhikevich, *Dynamical Systems in Neuroscience* (MIT Press, Cambridge, 2007).
[40] E. M. Izhikevich, IEEE Trans. Neural Netw. **15**, 1063 (2004).
[41] R. Krahe and F. Gabbian, Nat. Rev. Neurosci. **5**, 13 (2004).
[42] J. Lisman, Trends Neurosci. **20**, 38 (1997).
[43] E. N. Izhikevich, N. S. Desai, E. C. Walcott, and F. C. Hoppensteadt, Trends Neurosci. **26**, 161 (2003).
[44] B. W. Connors and M. J. Gutnick, Trends Neurosci. **13**, 99 (1990).
[45] C. M. Gray and D. A. McCormick, Science **274**, 109 (1996).
[46] R. L. Llinás and H. Jahnsen, Nature **297**, 406 (1982).
[47] D. A. McCormick and J. R. Huguenard, J. Neurophysiol. **8**, 1384 (1992).
[48] S. H. Lee, G. Govindaiah, and C. L. Cox, J. Physiol. **582**, 195 (2007).
[49] H. Su, G. Alroy, E. D. Kirson, and Y. Yaari, J. Neurosci. **21**, 4173 (2001).
[50] M. D. Womack and K. Khodakhah, J. Neurosci. **22**, 10603 (2002).
[51] T. R. Chay and J. Keizer, Biophys. J. **42**, 181 (1983).
[52] T. A. Kinard, G. de Vries, and A. Sherman, Biophys. J.

76, 1423 (1999).
[53] M. Pernarowski, R. M. Miura, and J. Kevorkian, SIAM J. Appl. Math. **52**, 1627 (1992).
[54] C. A. Del Negro, C.-F. Hsiao, S. H. Chandler, and A. Garfinkel, Biophys. J. **75**, 174 (1998).
[55] R. J. Butera, J. Rinzel, and J. C. Smith, J. Neurophysiol. **82**, 382 (1999).
[56] M. Steriade, D. A. McCormick, and T. J. Sejnowski, Science **262**, 679 (1993).
[57] M. Bazhenov and I. Timofevv, Scholarpedia **1(6)**, 1319 (2006).
[58] S. Gais, W. Plihal, U. Wagner, and J. Born, Nat. Neurosci. **3**, 1335 (2000).
[59] T. J. Sejnowski and A. Destexhe, Brain Res. **886**, 208 (2000).
[60] M. Bevan, P. Magill, D. Terman, J. Bolam, and C. Wilson, Trends Neurosci. **25**, 525 (2002).
[61] P. Brown, Cur. Opin. Neurobiol. **17**, 656 (2007).
[62] C. Park, R. M. Worth, and L. L. Rubchinsky, J. Neurophysiol. **103**, 2703 (2010).
[63] C. Hammond, H. Bergman, and P. Brown, Trends Neurosci. **30**, 357 (2007).
[64] P. J. Uhlhaas and W. Singer, Neuron **52**, 155 (2006).
[65] R. Fisher, W. van Emde Boas, W. Blume, C. Elger, P. Genton, P. Lee, and J. Engel, Epilepsia **46**, 470 (2005).
[66] V. N. Belykh, G. V. Osipov, V. S. Petrov, J. A. K. Suykens, and J. Vandewalle, Chaos **18**, 037106 (2008).
[67] S. J. Moon, K. A. Cook, K. Rajendran, K. G. Kevrekidis, J. Cisternas, and C. R. Liang, J. Math. Neurosci. **5**, 2 (2015).
[68] D. G. Aronson, M. Golubitsky, and M. Krupa, Nonlinearity **4**, 861 (1991).
[69] K. Wisenfeld, P. Colet, and S. Wisenfeld, Phys. Rev. Lett. **76**, 404 (1996).
[70] I. Z. Kiss, Y. Zhai, and H. Hudson, Phys. Rev. Lett. **94**, 248301 (2005).
[71] A. F. Taylor, P. Kapetanopoulos, B. J. Whitaker, R. Toth, L. Bull, and M. R. Tinsley, Phys. Rev. Lett. **100**, 214101 (2008).
[72] K. Miyakawa, T. Okano, and S. Yamazaki, J. Phy. Soc. Japan **82**, 034005 (2013).
[73] J. Zhang, Z. Yuan, and T. Zhou, Phys. Rev. E **79**, 041903 (2009).
[74] O. Sporns, *Networks of the Brain* (MIT Press, Cambridge, 2011).
[75] G. Buzsáki, C. Geisler, D. A. Henze, and X.-J. Wang, Trends Neurosci. **27**, 186 (2004).
[76] D. B. Chklovskii, B. W. Mel, and K. Svoboda, Nature **431**, 782 (2004).
[77] S. Song, P. J. Sjöström, M. Reigl, S. Nelson, and D. B. Chklovskii, PLoS Biol. **3**, e68 (2005).
[78] O. Sporns and C. J. Honey, Proc. Natl. Acad. Sci. USA **103**, 19219 (2006).
[79] P. Larimer and B. W. Strowbridge, J. Neurosci. **28**, 12212 (2008).
[80] E. Bullmore and O. Sporns, Nat. Rev. Neurosci. **10**, 186 (2009).
[81] O. Sporns, G. Tononi, and G. M. Edelman, Cereb. Cortex **10**, 127 (2000).
[82] D. S. Bassett and E. Bullmore, The Neuroscientist **12**, 512 (2006).
[83] P. Bonifazi, M. Goldin, M. A. Picardo, I. Jorquera, A. Cattani, G. Bianconi, A. Represa, Y. Ben-Ari, and R. Cossart, Science **326**, 1419 (2009).
[84] C. Wiedemann, Nat. Rev. Neurosci. **11**, 74 (2010).
[85] X. Li, G. Ouyang, A. Usami, Y. Ikegaya, and A. Sik, Biophys. J. **98**, 1733 (2010)
[86] R. J. Morgan and I. Soltesz, Proc. Natl. Acad. Sci. USA **105**, 6179 (2008).
[87] V. M. Eguíluz, D. R. Chialvo, G. A. Cecchi, M. Baliki, and A. V. Apkarian, Phys. Rev. Lett. **94**, 018102 (2005).
[88] M. P. Young, Philos. Trans. R. Soc. **252**, 13 (1993).
[89] M. P. Young, J. W. Scannell, G. A. Burns, and C. Blakemore, Rev. Neurosci. **5**, 227 (1994).
[90] J. W. Scannell, C. Blakemore, and M. P. Young, J. Neurosci. **15**, 1463 (1995).
[91] D. J. Felleman and D. C. Van Essen, Cereb. Cortex **1**, 1 (1991).
[92] J. W. Scannell, G. A. P. C. Burns, C. C. Hilgetag, M. A. O'Neill, and M. P. Young, Cereb. Cortex **9**, 277 (1999).
[93] O. Sporns, D. R. Chialvo, M. Kaiser, and C. C. Hilgetag, Trends Cogn. Sci. **8**, 418 (2004).
[94] M. Kaiser, R. Martin, P. Andras, and M. P. Young, Eur. J. Neurosci. **25**, 3185 (2007).
[95] A.-L. Barabási and R. Albert, Science **286**, 509 (1999).
[96] R. Albert and A.-L. Barabási, Rev. Mod. Phys. **74**, 47 (2002).
[97] J. L. Hindmarsh and R. M. Rose, Nature **296**, 162 (1982).
[98] J. L. Hindmarsh and R. M. Rose, Proc. R. Soc. London, Ser. B **221**, 87 (1984).
[99] R. M. Rose and J. L. Hindmarsh, Proc. R. Soc. London, Ser. B **225**, 161 (1985).
[100] A. Longtin, Phys. Rev. E **55**, 868 (1997).
[101] N. Brunel and X.-J. Wang, J. Neurophysiol. **90**, 415 (2003).
[102] M. San Miguel and R. Toral, in *Instabilities and Nonequilibrium Structures VI*, edited by J. Martinez, R. Tiemann, and E. Tirapegui (Kluwer Academic Publisher, Dordrecht, 2000), pp. 35-130.
[103] H. Shimazaki and S. Shinomoto, J. Comput. Neurosci. **29**, 171 (2010).